International Journal Of
Industrial Electronics Control and Optimization
Print ISSN: 3517-2645
Online ISSN: 3568-2645
Homepage: https://ieco.usb.ac.ir/

# Control of a shunt Active Power Filter with Voltage Source Model to Improve the Power Quality Performance

Mohammad Ali Heydari | Mahdi Hassanniakheibari | Gholamreza Sadeghi

Department of Electrical and Computer Engineering, University of Sistan and Baluchestan, Zahedan, Iran[1]
Department of Electrical Engineering, Zahedan Branch, Islamic Azad University, Zahedan, Iran[2]
Department of Electrical and Computer Engineering, Arak University of technology, Arak, Iran[3]
Corresponding author's email: mahdi.hassannia@iau.ac.ir

**Article Info**

**Article type:**
Research Article

**Article history:**
Received: 21-March-2024
Received in revised form: 03-July-2024
Accepted: 15-July-2024
Published online: 22-Sep-2024

**Keywords**:
Active Power Filter (APF),
Voltage Source Converter,
Error Dynamic,
Grid Harmonics,
Power Quality.

**ABSTRACT**

Active power filters (APFs) play a vital role in reducing the current harmonics and improving power quality. This work studies a shunt APF (SAPF) based on the three-phase voltage source converter (VSC). This paper investigates the new robust control approach using error dynamics. Stable first-order error dynamics are considered when designing the control inputs. Three control inputs are obtained to control the currents at any phase by choosing and optimizing the appropriate parameters. This strategy is also simple to implement in practical applications because it is the same as the proportional-derivative controller design. In addition, the new control method can be utilized for any system with low dynamic information so that the destructive effects of lumped uncertainties in the output channels of the SAPF can be alleviated. The minimum voltage and current measurements are used to control the SAPF, and the grid current harmonics will be reduced by achieving the stabilization of tracking error dynamics. Some numerical simulations are performed by MATLAB software to confirm the proposed method.

## I. Introduction

Electric energy loss is one of the most challenging issues in the power grid, and it can significantly impact its stability. The power grid losses are influenced by the impedance of transmission lines, which occur with the flow of current through them. If the load connected to the grid consumes reactive power, it causes an increase in losses and a decrease in the power transmission capacity of the lines. The proposed solution for these loads uses reactive power compensators, which large consumers usually utilize capacitors for compensation. The distribution grid uses compensators for small consumers at the beginning of feeder lines to solve this problem in the distribution lines and prevent them from reaching the transmission lines [1]-[3].

Technological advancements have led to the connection of loads to the grid that inject harmonic currents into it. Increasing these loads can significantly reduce the power transmission capacity and cause power plants to generate harmonic losses. In other words, power plants are built only for their outputs to be wasted and their costs to become irrecoverable. In this area, the harmonic compensator is an effective solution that can resolve the power grid's many crises [4]-[6].

Harmonics are also a critical problem in discussing power quality in distribution and transmission systems. Electricity companies must control the level of harmonic distortions in the grid and provide limitations to prevent damage to the equipment of residential and industrial customers. In most cases, voltage distortion is less than one percent in transmission systems, and as we get closer to the customers, the level of these distortions increases [7]-[10].

Distorted waveforms can be decomposed into a sum of the fundamental frequency and its harmonics. It is also common to use an index known as the total harmonic distortion (THD) to determine any waveform's distortion level. A higher value of the THD can lead to harmonic losses greater than the losses of the fundamental component. This failure can be solved by

Copyright © M. HassanniaKheibari.
Publisher: University of Sistan and Baluchestan

designing and implementing filters [11], [12].

Active Power Filters (APFs) are converters that generate compensating voltage and current as needed by using reactive instantaneous power and preventing harmonics from nonlinear loads from entering the grid. The main issue in this topic is how to control the converter for better and more accurate performance in compensating the grid's harmonic content. The APFs are classified into various categories, including their connection to the grid, type of converter, number of phases, modulation, and control methods [13]-[16].

Gyugyi and Strycula introduced shunt APFs (SAPFs) in 1976 [1]. These filters are an effective method for neutralizing harmonic currents from nonlinear loads. SAPFs are connected to the load and source in shunt. They monitor the current flow from the source to the load and generate a compensating current to neutralize harmonic content. SAPFs are typically used for low-power applications and filtering low-frequency harmonics. The advantage of SAPFs is their ease of implementation and their ability to have a fast response time [17].

The voltage source converter (VSC)s are generally used for low power levels, and the most important reason is the lower switching power loss compared to current source converters. Different models of VSC have been described in the literature. From this point of view, the VSC will be associated with unstructured uncertainties in the model. Therefore, dealing with uncertainties and the control of SAPF will become a controversial challenge. For this reason, a robust control method is required to deal with the lumped uncertainties in SAPF. Various control strategies for APFs have been reported in articles and research, including finite-set model predictive control [18], nonlinear control [19], adaptive sliding-mode backstepping control [20], neural network approach [21], [22], adaptive fuzzy control [23], [24], model-based control [25], and proportional-integral (PI) vector control [26]. In addition, the incorporation of robust control techniques that have been introduced in recent years can be considered for having the desired outputs in nonlinear systems. In other words, they can improve the design aspects and reduce the influence of destructive factors in the responses [27]-[31].

In [18], a finite-set model predictive control with coupling capacitor voltage observer scheme was proposed for thyristor-controlled LC-coupling hybrid APF. It ensures a fast transient response, low steady-state error, and good robustness under both inductive and capacitive load situations.

Research [19] introduces a nonlinear control technique for a three-phase APF. The control strategy includes a cascade structure of two loops. The inner-loop regulator is designed using the sliding mode control technique, and Lyapunov approaches to ensure the power factor correction objective by forcing the grid current to follow a given reference signal. The outer loop consists mainly of a PI regulator to regulate the output voltage. This scheme is implemented based on three control objectives:

- forcing the photovoltaic output voltage to track a reference signal provided by the maximum power point tracking block to produce their maximum power
- regulating the DC link voltage to satisfy the correct operation mode of the three-phase APF
- satisfying power factor correction objective at the point of common coupling

Recently, a novel hybrid two-loop nonlinear controller was designed for stabilization and robust control of the LCL-type SAPF in reference [20]. Backstepping, sliding mode, and adaptive controllers were combined to solve the closed-loop system's instability problem and the LCL coupling's inherent resonance in this work. The main objective of this strategy is to directly make the grid current in phase with the grid voltage.

In [21], an adaptive sliding mode reference model is proposed using a radial basis function neural network to control a single-phase APF. The neural network approximates the nonlinear function and eliminates modelling errors in the active power filter system. Moreover, a sliding mode voltage controller based on an exponential approach law is designed in reference [21] to improve the performance of AC side voltage tracking.

Research [22] proposes a new intelligent sliding-mode control approach to achieve harmonic suppression of an APF effectively. This work uses an intelligent complementary terminal sliding-mode controller to improve the control accuracy of the current loop and deal with the lumped disturbances in the system that are so attractive. In addition, a multiloop neural network, whose parameter learning laws are derived based on the Lyapunov laws, is proposed to approximate the unknown nonlinear function term in the APF dynamic model to reduce chattering.

In research [23], an adaptive fuzzy model reference control was studied to improve the dynamic performance of power, such as current tracking and THD for SAPFs. The fuzzy method was utilized to approximate the nonlinear model of the APF, which arises from nonlinear characteristics, variable parameters, and external disturbances. This study presents an adaptive fuzzy control system for the APF consisting of a Takagi-Sugeno fuzzy control part and a sliding mode control part, which can enhance the system's robust performance.

An adaptive fuzzy sliding mode control system is proposed in [24] to enhance the dynamic performance of a three-phase APF. Adaptive fuzzy systems are employed to approximate both the equivalent control term and the switching control term in the sliding mode controller. Thus, an online adaptive tuning algorithm for the subsequent parameters in the fuzzy rules is designed in [24]. Continuous switching control can somewhat reduce the phenomenon of chattering, and simulations conducted in [24] demonstrate that the proposed control method exhibits excellent dynamic performance, including

minor current tracking errors, reduction in THD, high robustness in the presence of parameter variations, and nonlinear loads.

Resilient model-based control for a three-phase SAPF is discussed in [25]. In the proposed control method in this study, a linear converter model is utilized, which is incorporated into the Kalman filter structure to estimate the system's state variables. Even though the estimated states in this method do not precisely match the real system variables, resulting in some error in their estimation, designing three sliding mode controllers is still feasible.

A PI vector control for controlling a hybrid LC APF system with ideal steady-state error, optimal transient response, and good robustness is presented in [26]. A transfer function for the proposed PI vector current controller is introduced in this research, and the parameter design for achieving an optimal transient response is discussed. Detailed analysis of the robustness of the PI vector current controller against system parameter variations, distorted grid voltages, and grid frequency variations is conducted.

This paper studies an SAPF based on the three-phase VSC and investigates the new robust control approach using error dynamics. When designing the control inputs, stable first-order error dynamics are considered. Three control inputs are obtained to control the currents at any phase by choosing and optimizing the appropriate parameters. This strategy is also simple to implement in practical applications because it is the same as the proportional-derivative controller design. In addition, the new control method can be utilized for any system with low dynamic information so that the destructive effects of lumped uncertainties in the output channels of the SAPF can be alleviated.

The rest of this paper is organized as follows: In Section II, the mathematical model of a SAPF is introduced. Discretization of the dynamic system is investigated in Section III. Section IV is dedicated to proposing the new robust control method. To verify the new proposed control scheme and investigation of the performance, a number of simulation results are provided in Section V. Finally, Section VI draws the conclusions.

## II. Model of the three-phase APF system

According to [25], an appropriate model of the three-phase APF was introduced, and this model is considered for the design of the proposed control scheme. Figure 1 shows the electrical circuit of the three-phase APF. The differential equations of this model are as follows:

$$\begin{aligned}
\frac{di_{F_a}(t)}{dt} &= -\frac{v_{dc}(t)}{2L_F}u_a(t)+\frac{v_{dc}(t)}{6L_F}(u_a(t)+u_b(t)+u_c(t))+\frac{v_a(t)}{L_F}\\
\frac{di_{F_b}(t)}{dt} &= -\frac{v_{dc}(t)}{2L_F}u_b(t)+\frac{v_{dc}(t)}{6L_F}(u_a(t)+u_b(t)+u_c(t))+\frac{v_b(t)}{L_F}\\
\frac{di_{F_c}(t)}{dt} &= -\frac{v_{dc}(t)}{2L_F}u_c(t)+\frac{v_{dc}(t)}{6L_F}(u_a(t)+u_b(t)+u_c(t))+\frac{v_c(t)}{L_F}\\
\frac{dv_{dc}(t)}{dt} &= \frac{i_{F_a}(t)u_a(t)}{2C}+\frac{i_{F_b}(t)u_b(t)}{2C}+\frac{i_{F_c}(t)u_c(t)}{2C}
\end{aligned} \tag{1}$$

where $i_{F_a}(t),i_{F_b}(t),i_{F_c}(t),v_{dc}(t)$ are the state variables, $u_a(t),u_b(t),u_c(t)$ are the control input commands which must be designed appropriately, and $v_a(t),v_b(t),v_c(t)$ are the voltages at the point of common coupling. In this paper, the main goal is the control of the system states to follow the references or $i^*_{F_a}(t),i^*_{F_b}(t),i^*_{F_c}(t),v^*_{dc}(t)$. In [25], by neglecting the effect of neutral-point voltage or

$$v_n(t)=\frac{v_{dc}(t)}{6}(u_a(t)+u_b(t)+u_c(t)) \tag{2}$$

a simple model has been achieved from (1). In other words, the voltage $v_n(t)$ is a high-frequency signal. This model is given by (3):

$$\begin{aligned}
\frac{di_{F_a}(t)}{dt} &= -\frac{v_{dc}(t)}{2L_F}u_a(t)+\frac{v_a(t)}{L_F}\\
\frac{di_{F_b}(t)}{dt} &= -\frac{v_{dc}(t)}{2L_F}u_b(t)+\frac{v_b(t)}{L_F}\\
\frac{di_{F_c}(t)}{dt} &= -\frac{v_{dc}(t)}{2L_F}u_c(t)+\frac{v_c(t)}{L_F}\\
\frac{dv_{dc}(t)}{dt} &= \frac{i_{F_a}(t)u_a(t)}{2C}+\frac{i_{F_b}(t)u_b(t)}{2C}+\frac{i_{F_c}(t)u_c(t)}{2C}
\end{aligned} \tag{3}$$

where $v_i(t),i=a,b,c$ are determined by (4):

$$\begin{aligned}
\frac{dv_i(t)}{dt} &= \omega_0 v_{iq}(t)\\
\frac{dv_{iq}(t)}{dt} &= -\omega_0 v_i(t)
\end{aligned} \tag{4}$$

and $\omega_0$ is the grid frequency.

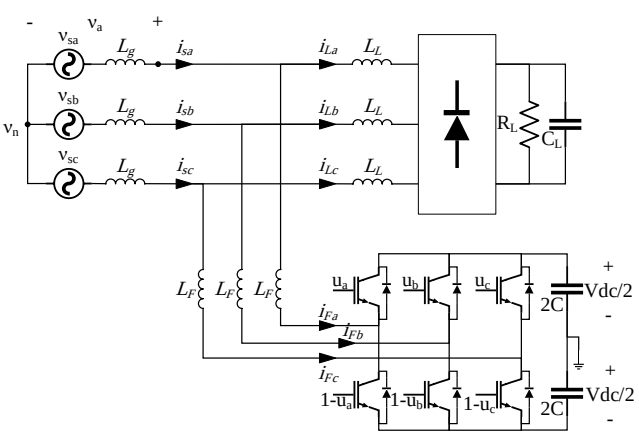



Fig. 1. The three-phase SAPF circuit connected to grid

## III. Discretization of the dynamic system

Consider the following approximation for the derivation of $f(x)$ related to $x$:

$$\frac{df(x)}{dx} \cong \frac{f(x+\Delta x)-f(x)}{\Delta x} \tag{5}$$

The step $\Delta x$ must be chosen very small. Nevertheless, the derivation computation process is long, and calculations in the microcontroller are done slowly.

Based on (5), a set of state equations described by (6) can be discretized.

$$\frac{dX(t)}{dt} = F(X(t),U(t),D(t)) \tag{6}$$

In (6), $X(t)=\left[x_1(t) \;\; x_2(t) \;\; \cdots \;\; x_n(t)\right]^T$ is the system state vector, $x_i(t), i=1,2,\cdots,n$ are the state variables, $F(\cdot)$ is the nonlinear function vector, $U(t)=\left[u_1(t) \;\; u_2(t) \;\; \cdots \;\; u_m(t)\right]^T$ is the control input vector, and $D(t)=\left[d_1(t) \;\; d_2(t) \;\; \cdots \;\; d_l(t)\right]^T$ is the disturbance vector.

Now, according to (5), the following expression is obtained for (6):

$$\begin{aligned} &\frac{dX(t)}{dt} \cong \frac{X(t+\Delta t)-X(t)}{\Delta t} = F(X(t),U(t),D(t)) \\ &X(t+\Delta t) = F(X(t),U(t),D(t))\Delta t + X(t) \end{aligned} \tag{7}$$

Therefore, by assigning the step $k$ and sampling time $T_s = 1/f_s$, the following result is concluded:

$$X(k+1) = F(X(k),U(k),D(k))T_s + X(k) \tag{8}$$

Based on (8), the dynamic model (3) or three-phase APF is discretized to model (9).

$$\begin{aligned} i_{F_a}(k+1) &= \left(-\frac{v_{dc}(k)}{2L_F}u_a(k)+\frac{v_a(k)}{L_F}\right)T_s + i_{F_a}(k) \\ i_{F_b}(k+1) &= \left(-\frac{v_{dc}(k)}{2L_F}u_b(k)+\frac{v_b(k)}{L_F}\right)T_s + i_{F_b}(k) \\ i_{F_c}(k+1) &= \left(-\frac{v_{dc}(k)}{2L_F}u_c(k)+\frac{v_c(k)}{L_F}\right)T_s + i_{F_c}(k) \\ v_{dc}(k+1) &= \left(\frac{i_{F_a}(k)u_a(k)+i_{F_b}(k)u_b(k)+i_{F_c}(k)u_c(k)}{2C}\right)T_s \\ &+ v_{dc}(k) \end{aligned} \tag{9}$$

where

$$\begin{aligned} v_i(k+1) &= \omega_0 v_{iq}(k)T_s + v_i(k) \\ v_{iq}(k+1) &= -\omega_0 v_i(k)T_s + v_{iq}(k) \end{aligned} \tag{10}$$

for $i = a,b,c$.

## IV. New robust controller design

Based on Fig. 1, by defining the tracking error as (11), the expressions (12) for error dynamics are obtained.

$$\begin{aligned} e_1(k) &= i_{S_a}(k) - i^*_{S_a}(k) = i_{F_a}(k) + i_{L_a}(k) - i^*_{S_a}(k) \\ e_2(k) &= i_{S_b}(k) - i^*_{S_b}(k) = i_{F_b}(k) + i_{L_b}(k) - i^*_{S_b}(k) \\ e_3(k) &= i_{S_c}(k) - i^*_{S_c}(k) = i_{F_c}(k) + i_{L_c}(k) - i^*_{S_c}(k) \\ e_4(k) &= v_{dc}(k) - v^*_{dc}(k) \end{aligned} \tag{11}$$

$$\begin{aligned} &e_1(k+1) = \\ &\left(-\frac{v_{dc}(k)}{2L_F}u_a(k)+\frac{v_a(k)}{L_F}\right)T_s + i_{F_a}(k) + i_{L_a}(k+1) - i^*_{S_a}(k+1) \\ &e_2(k+1) = \\ &\left(-\frac{v_{dc}(k)}{2L_F}u_b(k)+\frac{v_b(k)}{L_F}\right)T_s + i_{F_b}(k) + i_{L_b}(k+1) - i^*_{S_b}(k+1) \\ &e_3(k+1) = \\ &\left(-\frac{v_{dc}(k)}{2L_F}u_c(k)+\frac{v_c(k)}{L_F}\right)T_s + i_{F_c}(k) + i_{L_c}(k+1) - i^*_{S_c}(k+1) \\ &e_4(k+1) = \\ &\left(\frac{i_{F_a}(k)u_a(k)}{2C}+\frac{i_{F_b}(k)u_b(k)}{2C}+\frac{i_{F_c}(k)u_c(k)}{2C}\right)T_s + v_{dc}(k) - v^*_{dc} \end{aligned} \tag{12}$$

where $i^*_{S_a}(k), i^*_{S_b}(k), i^*_{S_c}(k)$ are grid currents references, $i_{L_a}(k), i_{L_b}(k), i_{L_c}(k)$ are load currents or disturbances and $v^*_{dc}(k)$ is constant or $v^*_{dc}(k)=v^*_{dc}$.

The error dynamic equations can be assumed as follows:

$$e_i(k+n) + \sum_{j=0}^{n-1}\gamma_{ji}e_i(k+j) = 0 \tag{13}$$

In (13), $\gamma_{ji}$ are the design parameters, and they are dependent on the number of steps. Due to the control inputs $u_a(k), u_b(k), u_c(k)$ are appreciated in the first step of the three-phase APF system equations; hence based on (13), the following relations can be written:

$$\begin{aligned} &e_1(k+1) + \gamma_{01}e_1(k) = 0 \\ &e_2(k+1) + \gamma_{02}e_2(k) = 0 \\ &e_3(k+1) + \gamma_{03}e_3(k) = 0 \\ &e_4(k+1) + \gamma_{04}e_4(k) = 0 \end{aligned} \tag{14}$$

Therefore, according to (12) and (14), a set of equations or (15) for designing the control inputs are the result. There are three control commands in (15), and no input exists for controlling the $v_{dc}(k)$. This failure can be resolved by adding three parameters as $K_{s1}(k), K_{s2}(k), K_{s3}(k)$, and assigning auxiliary input $u_{dc}(k)$ into $u_a(k), u_b(k), u_c(k)$.

$$\begin{aligned} \gamma_{01}e_1(k) &= -\left(-\frac{v_{dc}(k)}{2L_F}u_a(k)+\frac{v_a(k)}{L_F}\right)T_s - i_{F_a}(k) \\ &- i_{L_a}(k+1) + i^*_{S_a}(k+1) \\ \gamma_{02}e_2(k) &= -\left(-\frac{v_{dc}(k)}{2L_F}u_b(k)+\frac{v_b(k)}{L_F}\right)T_s - i_{F_b}(k) \\ &- i_{L_b}(k+1) + i^*_{S_b}(k+1) \\ \gamma_{03}e_3(k) &= -\left(-\frac{v_{dc}(k)}{2L_F}u_c(k)+\frac{v_c(k)}{L_F}\right)T_s - i_{F_c}(k) \\ &- i_{L_c}(k+1) + i^*_{S_c}(k+1) \\ \gamma_{04}e_4(k) &= -\left(\frac{i_{F_a}(k)u_a(k)+i_{F_b}(k)u_b(k)+i_{F_c}(k)u_c(k)}{2C}\right)T_s \\ &- v_{dc}(k) + v^*_{dc} \end{aligned} \tag{15}$$

In the following, firstly, control of the variables $i_{S_a}(k), i_{S_b}(k), i_{S_c}(k)$ is studied, and then the control of $v_{dc}(k)$ is investigated. Regarding (15), by dividing the first, second, and third equations by $\gamma_{01}, \gamma_{02}, \gamma_{03}$, (16) is obtained:

$$
\begin{aligned}
e_1(k) &= -\left(-\frac{v_{dc}(k)}{2\gamma_{01}L_F}u_a(k)+\frac{v_a(k)}{\gamma_{01}L_F}\right)T_s-\frac{i_{F_a}(k)}{\gamma_{01}}\\
&\quad -\frac{i_{L_a}(k+1)}{\gamma_{01}}+\frac{i_{S_a}^*(k+1)}{\gamma_{01}}\\
e_2(k) &= -\left(-\frac{v_{dc}(k)}{2\gamma_{02}L_F}u_b(k)+\frac{v_b(k)}{\gamma_{02}L_F}\right)T_s-\frac{i_{F_b}(k)}{\gamma_{02}}\\
&\quad -\frac{i_{L_b}(k+1)}{\gamma_{02}}+\frac{i_{S_b}^*(k+1)}{\gamma_{02}}\\
e_3(k) &= -\left(-\frac{v_{dc}(k)}{2\gamma_{03}L_F}u_c(k)+\frac{v_c(k)}{\gamma_{03}L_F}\right)T_s-\frac{i_{F_c}(k)}{\gamma_{03}}\\
&\quad -\frac{i_{L_c}(k+1)}{\gamma_{03}}+\frac{i_{S_c}^*(k+1)}{\gamma_{03}}
\end{aligned}
\tag{16}
$$

Consider the following control inputs:

$$
\begin{aligned}
u_a(k) &= \frac{2\gamma_{01}L_F}{T_s v_{dc}(k)}\left(K_{d1}e_1(k+1)+\left(K_{p1}+1\right)e_1(k)+T_sK_{s1}(k)u_{dc}(k)\right)\\
u_b(k) &= \frac{2\gamma_{02}L_F}{T_s v_{dc}(k)}\left(K_{d2}e_2(k+1)+\left(K_{p2}+1\right)e_2(k)+T_sK_{s2}(k)u_{dc}(k)\right)\\
u_c(k) &= \frac{2\gamma_{03}L_F}{T_s v_{dc}(k)}\left(K_{d3}e_3(k+1)+\left(K_{p3}+1\right)e_3(k)+T_sK_{s3}(k)u_{dc}(k)\right)
\end{aligned}
\tag{17}
$$

where $K_{di},K_{pi},i=1,2,3$ are the design parameters. Also, $u_{dc}(k)$ is an input for controlling the $v_{dc}(k)$. By substituting these relations into (16), (18) can be obtained:

$$
\begin{aligned}
e_1(k) &= K_{d1}e_1(k+1)+\left(K_{p1}+1\right)e_1(k)+T_sK_{s1}(k)u_{dc}(k)\\
&\quad -\frac{v_a(k)}{\gamma_{01}L_F}T_s-\frac{i_{F_a}(k)}{\gamma_{01}}-\frac{i_{L_a}(k+1)}{\gamma_{01}}+\frac{i_{S_a}^*(k+1)}{\gamma_{01}}\\
e_2(k) &= K_{d2}e_2(k+1)+\left(K_{p2}+1\right)e_2(k)+T_sK_{s2}(k)u_{dc}(k)\\
&\quad -\frac{v_b(k)}{\gamma_{02}L_F}T_s-\frac{i_{F_b}(k)}{\gamma_{02}}-\frac{i_{L_b}(k+1)}{\gamma_{02}}+\frac{i_{S_b}^*(k+1)}{\gamma_{02}}\\
e_3(k) &= K_{d3}e_3(k+1)+\left(K_{p3}+1\right)e_3(k)+T_sK_{s3}(k)u_{dc}(k)\\
&\quad -\frac{v_c(k)}{\gamma_{03}L_F}T_s-\frac{i_{F_c}(k)}{\gamma_{03}}-\frac{i_{L_c}(k+1)}{\gamma_{03}}+\frac{i_{S_c}^*(k+1)}{\gamma_{03}}
\end{aligned}
\tag{18}
$$

**Remark 1** *To achieve the desirable control of the three-phase APF, it is important the control of* $v_{dc}(k)$. *In other words, this issue affects the control procedure of the other state variables. For this reason, the weighted coefficients* $K_{s1}(k),K_{s2}(k),K_{s3}(k)$ *are considered to decrease the destructive effects of the* $u_{dc}(k)$. *This strategy can lead to satisfactory tracking and less ripple in the state variables and system outputs.*

Rearranging the (18) and dividing the error dynamics by $K_{d1},K_{d2},K_{d3}$, (19) one gets:

$$
\begin{aligned}
e_1(k+1) &= -\frac{K_{p1}}{K_{d1}}e_1(k)+\varepsilon_1(k)\\
e_2(k+1) &= -\frac{K_{p2}}{K_{d2}}e_2(k)+\varepsilon_2(k)\\
e_3(k+1) &= -\frac{K_{p3}}{K_{d3}}e_3(k)+\varepsilon_3(k)
\end{aligned}
\tag{19}
$$

where

$$
\begin{aligned}
\varepsilon_1(k) &= \frac{v_a(k)}{\gamma_{01}K_{d1}L_F}T_s+\frac{i_{F_a}(k)+i_{L_a}(k+1)-i_{S_a}^*(k+1)}{\gamma_{01}K_{d1}}\\
&\quad -\frac{T_sK_{s1}(k)}{K_{d1}}u_{dc}(k)\\
\varepsilon_2(k) &= \frac{v_b(k)}{\gamma_{02}K_{d2}L_F}T_s+\frac{i_{F_b}(k)+i_{L_b}(k+1)-i_{S_b}^*(k+1)}{\gamma_{02}K_{d2}}\\
&\quad -\frac{T_sK_{s2}(k)}{K_{d2}}u_{dc}(k)\\
\varepsilon_3(k) &= \frac{v_c(k)}{\gamma_{03}K_{d3}L_F}T_s+\frac{i_{F_c}(k)+i_{L_c}(k+1)-i_{S_c}^*(k+1)}{\gamma_{03}K_{d3}}\\
&\quad -\frac{T_sK_{s3}(k)}{K_{d3}}u_{dc}(k)
\end{aligned}
\tag{20}
$$

We consider the $\varepsilon_1(k),\varepsilon_2(k),\varepsilon_3(k)$ are lumped uncertainties in the error dynamics. According to (20), if the parameters $\gamma_{01},\gamma_{02},\gamma_{03}$ and $K_{d1},K_{d2},K_{d3}$ be the large numbers, then the destructive effects of $v_i(k)$, $i_{Fi}(k)$, $i_{Li}(k+1)$, $i^*_{si}(k+1)$, $u_{dc}(k)$, $i=a,b,c$ in $\varepsilon_1(k),\varepsilon_2(k),\varepsilon_3(k)$ can be attenuated. Hence, $\varepsilon_1(k),\varepsilon_2(k),\varepsilon_3(k)$ in (20) can be considered weak perturbations. Finally, by tuning the parameters $K_{p1},K_{p2},K_{p3}$, the stability of the error dynamics is guaranteed, and tracking errors $e_1(k),e_2(k),e_3(k)$ can be set near to zero by increasing step $k$. For stabilizing (19), $K_{di},K_{pi},i=1,2,3$ must be chosen as follows:

$$
\frac{K_{p1}}{K_{d1}}>0,\frac{K_{p2}}{K_{d2}}>0,\frac{K_{p3}}{K_{d3}}>0 \tag{21}
$$

Now the design of $u_{dc}(k)$ for controlling the state variable $v_{dc}(k)$ is investigated. Based on the fourth equation in (15), and according to the definition of inputs in (17), the following expression can be obtained:

$$
\begin{aligned}
e_4(k) &= -\frac{L_FT_s}{\gamma_{04}Cv_{dc}(k)}\left(\gamma_{01}i_{F_a}(k)K_{s1}(k)+\gamma_{02}i_{F_b}(k)K_{s2}(k)\right.\\
&\quad \left.+\gamma_{03}i_{F_c}(k)K_{s3}(k)\right)u_{dc}(k)-\varepsilon_4(k)
\end{aligned}
\tag{22}
$$

where

$$
\begin{aligned}
\varepsilon_4(k) &= \frac{\gamma_{01}L_Fi_{F_a}(k)}{\gamma_{04}Cv_{dc}(k)}\left(K_{d1}e_1(k+1)+\left(K_{p1}+1\right)e_1(k)\right)\\
&\quad +\frac{\gamma_{02}L_Fi_{F_b}(k)}{\gamma_{04}Cv_{dc}(k)}\left(K_{d2}e_2(k+1)+\left(K_{p2}+1\right)e_2(k)\right)\\
&\quad +\frac{\gamma_{03}L_Fi_{F_c}(k)}{\gamma_{04}Cv_{dc}(k)}\left(K_{d3}e_3(k+1)+\left(K_{p3}+1\right)e_3(k)\right)\\
&\quad +\frac{v_{dc}(k)}{\gamma_{04}}-\frac{v_{dc}^*}{\gamma_{04}}
\end{aligned}
\tag{23}
$$

If the parameter $\gamma_{04}$ be a large number enough, then it is clear that the destructive effect of $\varepsilon_4(k)$ can be neglected in (22), or alternatively $\varepsilon_4(k)$ is a weak perturbation. Consequently, by supposing the $u_{dc}(k)$ as proposed in (24), the new error dynamic (25) will be constructed:

$$
\begin{aligned}
u_{dc}(k) &= -\frac{\gamma_{04}Cv_{dc}(k)}{L_FT_s}\times\\
&\quad \frac{\left(K_{d4}e_4(k+1)+\left(K_{p4}+1\right)e_4(k)\right)}{\left(\gamma_{01}i_{F_a}(k)K_{s1}(k)+\gamma_{02}i_{F_b}(k)K_{s2}(k)+\gamma_{03}i_{F_c}(k)K_{s3}(k)\right)}
\end{aligned}
\tag{24}
$$

$$e_4(k+1) = -\frac{K_{p4}}{K_{d4}} e_4(k) + \varepsilon_4(k) \quad (25)$$

Finally, by choosing the $K_{p4}$ appropriately, the tracking error $e_4(k)$ is set near to zero, and $v_{dc}(k)$ follows the reference signal $v_{dc}^*$. Accordingly, the stabilization of the error dynamic (25) is guaranteed by considering the following inequality:

$$\frac{K_{p4}}{K_{d4}} > 0 \quad (26)$$

## V. Simulation results

The new controller is simulated by MATLAB software to confirm the performance of the three-phase APF and analyze the electrical circuit outputs. For simulating the nonlinear load, a three-phase diode rectifier connected with a resistor load has been employed, and the grid current references are constructed as $i_{Si}^*(k)=u_{dc}(k)v_i(k)$. The APF switches are IGBT type in the shunt form with inverse diode. In addition, the power circuit has some voltage and current measurements.

Generally, the distribution grid load is defined in an interval between minimum and maximum modes or cases. It is clear that minimum and maximum intervals are also considered for linear loads, and the performance of the APF is studied at this interval—moreover, the diode bridge resistor load changes between two currents, 8A and 16A.

The parameter values for simulation are $\gamma_{01} = \gamma_{02} = \gamma_{03} = \gamma_{04} = 100$, $K_{p1}=K_{p2}=K_{p3} = 100$, $K_{d1}=K_{d2}=K_{d3} = 10$, and $K_{s1}(k)=K_{s2}(k)=K_{s3}(k) = 1$. The circuit parameter values are $v_s = 220V$, $v_{dc} = 400V$, $L_F = 5mH$, $C = 1500\mu F$, $f_{switching} = 10KHz$, $f_s = 20KHz$.

### A. The maximum current case

In this case, the diode bridge resistor load is considered 24Ω with a grid current of 16A and a THD of 26.69%. Fig. 2 illustrates the current harmonic frequency spectrum for the nonlinear load.

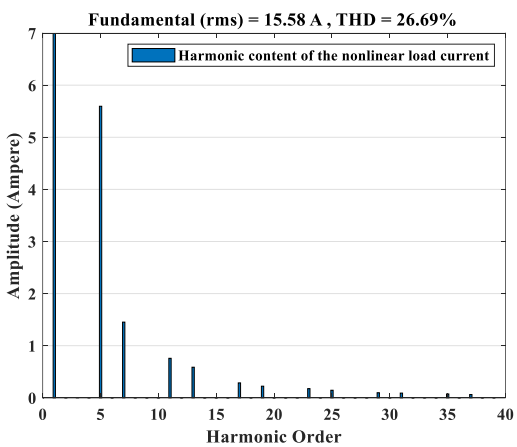



Fig. 2. The harmonic frequency spectrum for the nonlinear load current in the maximum case

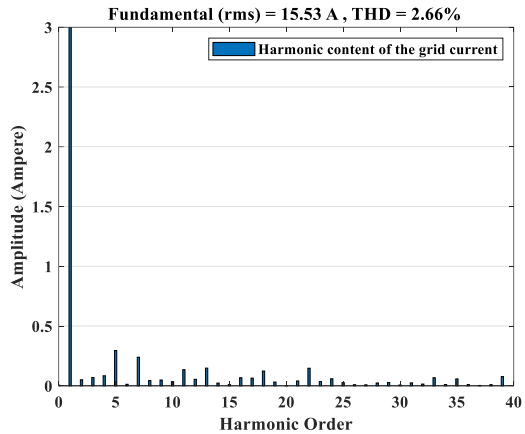



Fig. 3. The harmonic frequency spectrum for the nonlinear load current in the maximum case with existing the SAPF

After connecting the SAPF to the grid, the grid harmonic content is decreased based on Fig. 3. In this case, the amount of THD is reduced to 2.66%, an admissible value.

Fig. 4-a shows the waveform of the nonlinear current load constructed by the bridge diode. By connecting the SAPF to the grid, the grid current is as Fig. 4-b. To remove the nonlinear current harmonics from the grid current, the filter current should be as Fig. 4-c. In this simulation, the DC link capacitor's reference voltage is 400V, shown in Fig. 4-d.

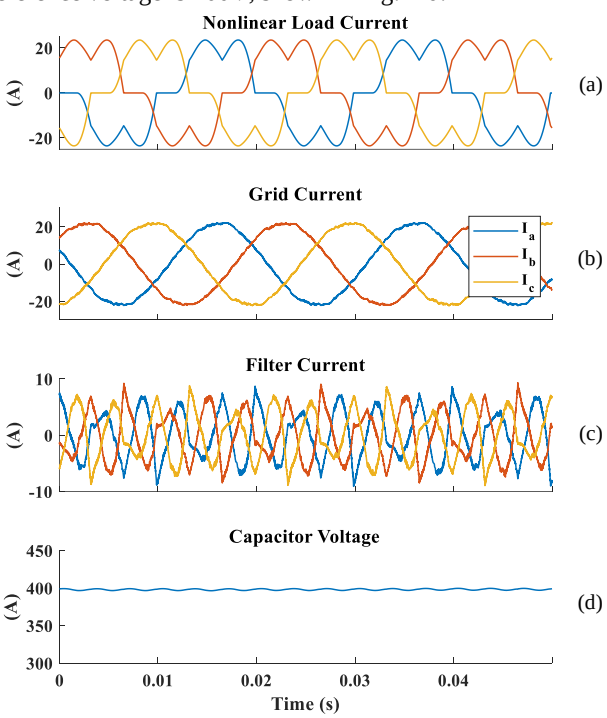



Fig. 4. The simulation results of the SAPF with nonlinear load constructed by diode bridge. (a) The waveform of the nonlinear load current (b) The waveform of the grid current after connecting the SAPF (c) The waveform of the SAPF (d) The waveform of the DC link capacitor voltage

### B. The minimum current case

The minimum current for a nonlinear load can be obtained by considering a 48Ω resistor instead of 24Ω in the output of

the bridge diode. The harmonic frequency spectrum is depicted in Fig. 5.

TABLE I
THE COMPARISON AMONG DIFFERENT CONTROLLERS FOR APF

| Controller | [18] | [19] | [20] | [21] | [22] | [23] | [24] | [25] | [26] | Proposed |
|---|---|---|---|---|---|---|---|---|---|---|
| Year | 2023 | 2022 | 2023 | 2015 | 2023 | 2015 | 2013 | 2016 | 2021 | This work |
| Design complexity | Low | Low | Medium | High | High | Medium | low | Low | Medium | Low |
| Practical implementation | Medium | Medium | Hard | Hard | Medium | Hard | Medium | Simple | Medium | Simple |
| Dynamic model information | Yes | Yes | Yes | No | Yes | Yes | Yes | Yes | Yes | No |
| Robustness | Medium | Weak | Weak | Medium | Medium | Medium | Medium | Medium | Weak | High |
| Confrontation with uncertainty | Indirect | Indirect | Indirect | Indirect | Indirect | Indirect | Indirect | Indirect | Indirect | Direct |
| Steady-state accuracy | High | High | Medium | Medium | High | Medium | Medium | High | High | Medium |
| Transient response speed | Fast | Slow | Fast | Medium | Medium | Fast | Fast | Fast | Fast | Fast |

In the case of minimum current, the amount of current is $8A$ , and THD is 36.52%. Naturally, this THD is greater than that from the maximum current case. Based on Fig. 6, employing the SAPF reduces the amount of THD for grid current to 3.73%.

In Fig. 7, the waveforms of the nonlinear load at minimum current mode, the grid current with the SAPF already in the grid, the SAPF current, and the DC link capacitor voltage have been demonstrated to be similar to the maximum mode.

These results are confirmed in the minimum case, and the performance of the control approach is verified.

Finally, the comparison among different controllers designed in references [18]-[26] for APF has been tabulated in Table I. According to Table I, several aspects of the controllers introduced in previous works are investigated. A number of factors are explained in this table, for example, the design complexity, practical implementation, the amount of dynamic model information for design, robustness, and confrontation with uncertainty of the controllers. Also, the steady-state accuracy and the transient response speed for methods are compared.

Based on Table I and the comparison between the other methods provided in [18]-[26], it is clear that the proposed approach has a simple design. In other words, the tuning of parameters $K_{pi}$,$K_{di}$,$\gamma_{0i}$ is necessary, according to the level of uncertainties and control objects. The robustness ratio can be regulated using $\gamma_{0i}$. In addition, unlike the other methods, we can deal with lumped uncertainties directly. Also, in the design of the proposed method, the dynamic model information is not necessary. These issues are the advantages of the proposed method over the other approaches.

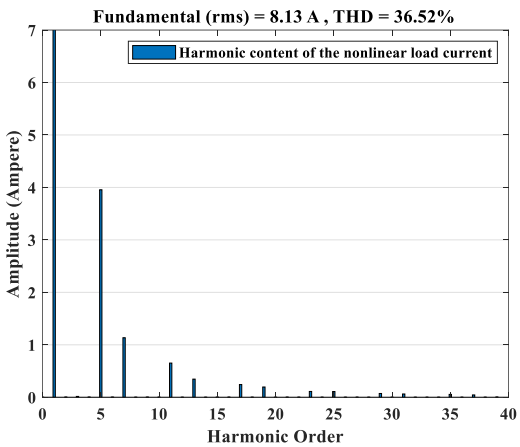



Fig. 5. The harmonic frequency spectrum for the nonlinear load current in the minimum case

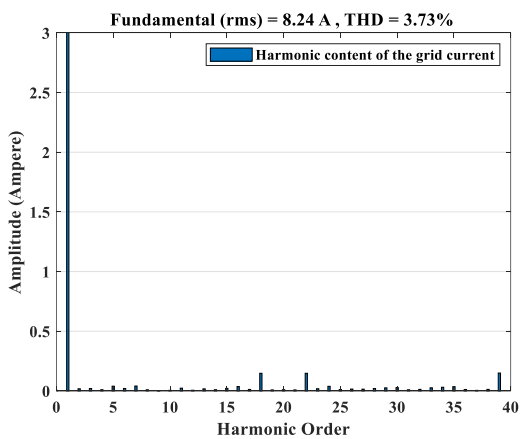



Fig. 6. The harmonic frequency spectrum for the nonlinear load current in the minimum case with existing the SAPF

## VI. Conclusion

This paper takes into account the SAPF based on the three-phase current source converter. According to error dynamics, a new robust control method was introduced in this paper, and numerical simulation with experimental results were provided. The robust control approach is simple to implement in practical situations. This control method is fast, in contrast to other methods. Also, this approach is highly robust compared to the variation of the parameters and unmolded dynamics. The

simulation results explicated the satisfactory performance of the SAPF in compensating the harmonics.

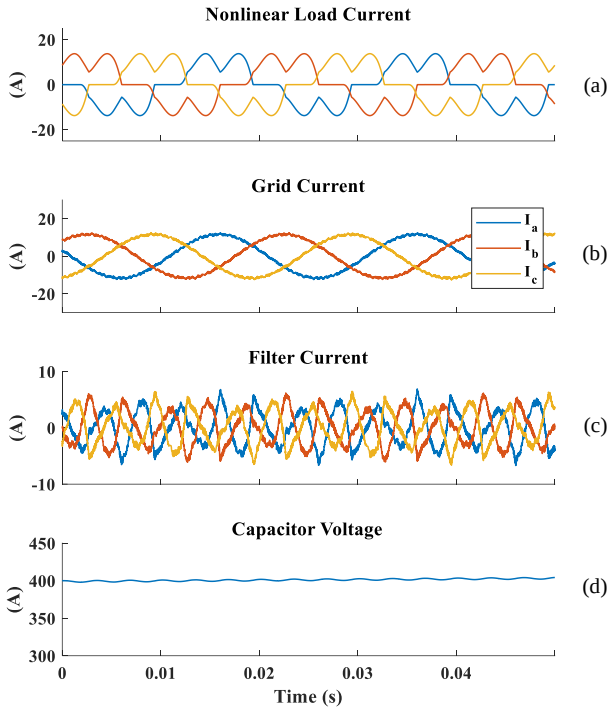



Fig. 7. The simulation results of the SAPF with nonlinear load constructed by diode bridge. (a) The waveform of the nonlinear load current (b) The waveform of the grid current after connecting the SAPF (c) The waveform of the SAPF (d) The waveform of the DC link capacitor voltage.

## REFERENCES


[1] F. Blaabjerg, Control of Power Electronic Converters and Systems: Volume 2, 1st edit. Elsevier, 2018.

[2] A. Terciyanli et al., "A Current Source Converter-Based Active Power Filter for Mitigation of Harmonics at the Interface of Distribution and Transmission Systems," IEEE Trans. Ind. Appl., vol. 48, no. 4, pp. 1374–1386, Jul. 2012, doi: 10.1109/TIA.2012.2200009.

[3] N. Bagheri, H. Alipour, L. Mohammadian, J. Beiza, and M. Ebadpour, "A Multiport isolated resonant LLC converter for grid-tied renewable energy powered bidirectional EV charger," International Journal of Industrial Electronics Control and Optimization (IECO), vol. 6, no. 1, pp.37-48, 2023.

[4] B. Singh, K. Al-Haddad, and A. Chandra, "A review of active filters for power quality improvement," IEEE Trans. Ind. Electron., vol. 46, no. 5, pp. 960–971, 1999, doi: 10.1109/41.793345.

[5] A. Govind, V. Kumar Tayal, and R. K. Kumawat, "Comparison of Current Controlling Methods for Shunt Active Power Filters to Improve Power Quality," in 2022 10th International Conference on Reliability, Infocom Technologies and Optimization (Trends and Future Directions) (ICRITO), Oct. 2022, no. Lc, pp. 1–5, doi: 10.1109/ICRITO56286.2022.9965182.

[6] M. Sabarimuthu, N. Senthilnathan, N. Priyadharshini, M. A. Kumar, N. Telagam, and S. K. Sree, "Comparison of Current Control Methods for a Three Phase Shunt Active Filter," in 2021 7th International Conference on Electrical Energy Systems (ICEES), Feb. 2021, pp. 32–37, doi: 10.1109/ICEES51510.2021.9383754.

[7] H. Akagi, "New trends in active filters for power conditioning," IEEE Trans. Ind. Appl., vol. 32, no. 6, pp. 1312–1322, 1996, doi: 10.1109/28.556633.

[8] J. Afonso, C. Couto, and J. Martins, "Active Filters with Control Based on the p-q Theory," IEEE Ind. Electron. Soc., vol. 47, no. May 2014, pp. 5–10, 2000, [Online]. Available: http://hdl.handle.net/1822/1921.

[9] Z. Xiao, H. Xue, T. Liu, and G. Zheng, "Research on Control Strategy of Shunt Active Power Filter," in 2023 8th Asia Conference on Power and Electrical Engineering (ACPEE), Apr. 2023, pp. 2377–2382, doi: 10.1109/ACPEE56931.2023.10135649.

[10] C. Ranga Rao, R. Balamurugan, and R. Alla, "Synchronization control techniques for shunt active power filter: an overview," Bull. Electr. Eng. Informatics, vol. 12, no. 1, pp. 1–9, Feb. 2023, doi: 10.11591/eei.v12i1.4300.

[11] M. Miletić, K. R. Raguž, V. Zeleničić, I. Erceg, and D. Sumina, "Development of Single-Phase Shunt Active Power Filter for Reduction of Current Harmonics in Data Center Power System," in 2023 11th International Conference on Smart Grid (icSmartGrid), Jun. 2023, pp. 1–7, doi: 10.1109/icSmartGrid58556.2023.10170839.

[12] R. Hou, P. Wang, J. Wu, and D. Xu, "Research on Oscillation Suppression Methods in Shunt Active Power Filter System," Energies, vol. 15, no. 9, 2022, doi: 10.3390/en15093125.

[13] L. Zhou, Z. Zhou, J. Qi, and W. Han, "Hybrid Prediction-Based Deadbeat Control for a High-Performance Shunt Active Power Filter," IEEE Access, vol. 11, no. January, pp. 11118–11131, 2023, doi: 10.1109/ACCESS.2023.3241300.

[14] J.-H. Urrea-Quintero, N. Muñoz-Galeano, and J. M. López-Lezama, "Robust Control of Shunt Active Power Filters: A Dynamical Model-Based Approach with Verified Controllability," Energies, vol. 13, no. 23, p. 6253, Nov. 2020, doi: 10.3390/en13236253.

[15] H. Sadeghi, and H.R. Mohammadi, "An improved fuzzy controlled back-to-back electric spring using hybrid structure of ES-1 and shunt-APF to improve power quality in microgrids," International Journal of Industrial Electronics Control and Optimization (IECO), vol. 5, no. 1, pp.89-98, 2022.

[16] T. Toumi, A. Allali, A. Meftouhi, O. Abdelkhalek, A. Benabdelkader, and M. Denai, "Robust control of series active power filters for power quality enhancement in distribution grids: Simulation and experimental validation," ISA Trans., vol. 107, no. xxxx, pp. 350–359, 2020, doi: 10.1016/j.isatra.2020.07.024.

[17] A. Munduate, G. Garcera, and E. Figueres, "Robust control of a Shunt Active Power Filter for the medium voltage range based on a three-level Neutral Point Clamped converter," in IECON 2006 - 32nd Annual Conference on IEEE Industrial Electronics, Nov. 2006, pp. 2162–2167, doi: 10.1109/IECON.2006.347274.

[18] W.-K. Sou, P.-I. Chan, C. Gong, and C.-S. Lam, "Finite-Set Model Predictive Control for Hybrid Active Power Filter," IEEE Transactions on Industrial Electronics, vol. 70, no. 1, pp. 52–64, Jan. 2023, doi: 10.1109/tie.2022.3146550.

[19] A. Elallali, A. Abouloifa, I. Lachkar, C. Taghzaoui, F. Giri, and Y. Mchaouar, "Nonlinear control of grid-connected PV

systems using active power filter with three-phase three-level NPC inverter," IFAC-PapersOnLine, vol. 55, no. 12, pp. 61–66, 2022, doi: 10.1016/j.ifacol.2022.07.289.
[20] V. Hajbani, A. Zakipour, and M. Salimi, "A novel Lyapunov-based robust controller design for LCL-type shunt active power filters using adaptive sliding-mode backstepping approach," e-Prime - Advances in Electrical Engineering, Electronics and Energy, vol. 5, p. 100200, Sep. 2023, doi: 10.1016/j.prime.2023.100200.
[21] Y. Fang, J. Fei, and K. Ma, "Model reference adaptive sliding mode control using RBF neural network for active power filter," Int. J. Electr. Power Energy Syst., vol. 73, pp. 249–258, Dec. 2015, doi: 10.1016/j.ijepes.2015.05.009.
[22] L. Zhang and J. Fei, "Intelligent Complementary Terminal Sliding Mode Using Multiloop Neural Network for Active Power Filter," IEEE Transactions on Power Electronics, vol. 38, no. 8, pp. 9367–9383, Aug. 2023, doi: 10.1109/tpel.2023.3266738.
[23] K. Ma and J. Fei, "Model reference adaptive fuzzy control of a shunt active power filter," J. Intell. Fuzzy Syst., vol. 28, no. 1, pp. 485–494, 2015, doi: 10.3233/IFS-141325.
[24] S. Hou and J. Fei, "Adaptive fuzzy sliding control with fuzzy sliding term for three-phase active power filter," in 2013 10th IEEE International Conference on Control and Automation (ICCA), Jun. 2013, no. 2612012, pp. 1318–1323, doi: 10.1109/ICCA.2013.6564895.
[25] R. Guzman, L. G. de Vicuna, J. Morales, M. Castilla, and J. Miret, "Model-Based Control for a Three-Phase Shunt Active Power Filter," IEEE Trans. Ind. Electron., vol. 63, no. 7, pp. 3998–4007, Jul. 2016, doi: 10.1109/TIE.2016.2540580.
[26] C. Gong, W.-K. Sou, and C.-S. Lam, "Design and Analysis of Vector Proportional–Integral Current Controller for LC-Coupling Hybrid Active Power Filter With Minimum DC-Link Voltage," IEEE Trans. Power Electron., vol. 36, no. 8, pp. 9041–9056, Aug. 2021, doi: 10.1109/TPEL.2021.3049834.
[27] A. Zarei, M. S. Poutari, and S. M. Barakati, "Trajectory tracking for two-degree of freedom helicopter system using a controller-disturbance observer integrated design," ISA Transactions, vol. 74, pp. 99–110, Mar. 2018, doi: 10.1016/j.isatra.2017.12.026.
[28] A. Zarei, Y. Mousavi, R. Mosalanezhad, and M. H. Atazadegan, "Robust Voltage Control in Inverter-Interfaced Microgrids Under Plug-and-Play Functionalities," IEEE Systems Journal, vol. 14, no. 2, pp. 2813–2824, Jun. 2020, doi: 10.1109/jsyst.2019.2956684.
[29] Y. Mousavi, A. Zarei, and Z. S. Jahromi, "Robust adaptive fractional-order nonsingular terminal sliding mode stabilization of three-axis gimbal platforms," ISA Transactions, vol. 123, pp. 98–109, Apr. 2022, doi: 10.1016/j.isatra.2021.05.027.
[30] A. Zarei and S. Tavakoli, "Lumped uncertainty alleviation in output channels of MIMO nonlinear systems based on robust disturbance observer-based control strategy," Asian Journal of Control, vol. 25, no. 3, pp. 2001–2011, May 2022, doi: 10.1002/asjc.2834.
[31] A. Hassannia, S. M. Barakati, and S. H. Torabi, "Robust discrete sliding mode controller design for a single-phase onboard integrated electric vehicle charger with disturbance estimation," Computers and Electrical Engineering, vol. 110, p. 108881, Sep. 2023, doi: 10.1016/j.compeleceng.2023.108881.



**Mohammad Ali Heydari**; received his M.Sc in Electrical engineering from Sajjad Mashhad University of Technology, Mashahd, Iran in 2015 and Ph.D degree in Electrical engineering at University of Sistan and Baluchestan, Zahedan, Iran.



**Mahdi Hassanniakheibari** was born in Gonabad, Iran, in 1987. He received his PhD in Power Electrical Engineering from the Islamic Azad University, Science and Research Branch, Tehran, Iran, in 2020. He is an Assistant Professor at the Islamic Azad University, Zahedan Branch. His research interests include power systems, distribution networks, demand response, and power electronic converters.



**Gholamreza Sadeghi**; received his B.Sc degree in Electrical engineering from Imam Ali university, Iran in 2009. Now he is pursuing M.Sc degree in power electronic at the Arak University of technology, Arak, Iran.